Quality Improvement Study

Medicine®

OPEN

# Evaluation of three-dimensional iterative image reconstruction in C-arm-based interventional cone-beam CT

## A phantom study in comparison with customary reconstruction technique

Shigeru Suzuki, MD, PhD[a,*], Yoshiaki Katada, MD, PhD[a], Tomoko Takayanagi, MD[a,b], Haruto Sugawara, MD[a,b], Takuya Ishikawa, MD[a], Yuzo Yamamoto, RT[a], Hiroo Wada, MD, PhD, FACP[c]

**Abstract**

We compared images obtained using a three-dimensional iterative image reconstruction (3D-IIR) algorithm for C-arm-based interventional cone-beam computed tomography (CBCT) with that using the customary reconstruction technique to quantify the effect of reconstruction techniques on image quality.

We scanned 2 phantoms using an angiography unit with digital flat-panel system—an elliptical cylinder acrylic phantom to evaluate spatial resolution and a Catphan phantom to evaluate CT number linearity, image noise, and low-contrast resolution. Three-dimensional imaging was calculated using Feldkamp algorithms, and additional image sets were reconstructed using 3D-IIR at 5 settings (Sharp, Default, Soft+, Soft++, Soft+++). We evaluated quality of images obtained using the 6 reconstruction techniques and analyzed variance to test values of the 10% value of each MTF, mean CT number, and contrast-to-noise ratio (CNR), with $P < .05$ considered statistically significant.

Modulation transfer function curves and CT number linearity among images obtained using the customary technique and the 5 3D-IIR techniques showed excellent agreement. Noise power spectrum curves demonstrated uniform noise reduction across the spatial frequency in the iterative reconstruction, and CNR obtained using all but the Sharp 3D-IIR technique was significantly better than that using the customary reconstruction technique (Sharp, $P = .1957$; Default, $P = .0042$; others, $P < .0001$). Use of 3D-IIR, especially the Soft++ and Soft+++ settings, improved visualization of low-contrast targets.

Use of a 3D-IIR can significantly improve image noise and low-contrast resolution while maintaining spatial resolution in C-arm-based interventional CBCT, yielding higher quality images that may increase safety and efficacy in interventional radiology.

**Abbreviations:** 3D = three-dimensional, 3D-IIR = three-dimensional iterative image reconstruction, CBCT = cone-beam computed tomography, CNR = contrast-to-noise ratio, CT = computed tomography, FBP = filtered back projection, FPD = flat-panel detector, IR = iterative reconstruction, MTF = modulation transfer function, $MTF_{10}$%=10% value of modulation transfer function, NPS = noise power spectrum.

**Keywords:** angiography, experimental studies, image reconstruction, image-based iterative reconstruction

## 1. Introduction

Recently developed angiography systems with a flat-panel detector (FPD) allow acquisition of computed tomography (CT)-like cross-sectional images—C-arm-based cone-beam CT images (CBCT),[1–4] and new imaging methods have been investigated for CBCT.[5–7] C-arm-based CBCT setups are classified into 2 types: C-arm-based interventional CBCT systems and dedicated C-arm-based CBCT systems for dental, head and neck, extremity imaging, and mammography.[8] C-arm-based interventional CBCT images aid minimally invasive imaging-guided interventions.[2,9–16] However, the quality of these C-arm-based CBCT images is inferior to that of images obtained using conventional CT, especially with regard to contrast resolution.[2,17–19] Improved image quality with less noise than that obtained using customary filtered back projection (FBP) has been reported utilizing iterative reconstruction (IR) algorithms in conventional CT.[20,25] Also, the usefulness of IR techniques for dedicated C-arm-based CBCT imaging have been reported.[26,27] However, IR algorithms have not been widely applied in the acquisition of C-arm-based interventional CBCT images in clinical settings. Nevertheless, their adaptation in the acquisition of C-arm-based interventional CBCT images is expected to improve image quality similarly to their use in conventional CT imaging.

We compared the images obtained using three-dimensional iterative image reconstruction (3D-IIR)—an image-based IR algorithm—in C-arm-based interventional CBCT with those acquired using the customary reconstruction technique to determine the usefulness of the IR algorithm in improving the image quality.

*Editor: Pierleone Lucatelli.*

*The authors have no funding and conflicts of interest to disclose.*

*[a] Department of Radiology, Tokyo Women's Medical University Medical Center East, Arakawa-ku, [b] Department of Radiology, Graduate School of Medicine, University of Tokyo, Bunkyo-ku, [c] Department of Public Health, Graduate School of Medicine, Juntendo University, Bunkyo-ku, Tokyo, Japan.*

*[*] Correspondence: Shigeru Suzuki, Department of Radiology, Tokyo Women's Medical University Medical Center East, 2-1-10 Nishiogu, Arakawa-ku, Tokyo 116-8567, Japan (e-mail: shig.suz@gmail.com).*



*Medicine (2019) 98:13(e14947)*

*Received: 3 June 2018 / Received in final form: 23 December 2018 / Accepted: 24 February 2019*

*http://dx.doi.org/10.1097/MD.0000000000014947*

## 2. Materials and methods

Ethical approval was not necessary because this was a phantom study.

### 2.1. Phantoms

To quantify the effect of reconstruction techniques on image quality, we evaluated spatial resolution in images of an elliptical cylinder acrylic phantom and assessed CT number linearity, system noise, and low-contrast resolution using a Catphan 500 phantom (The Phantom Laboratory, Greenwich, NY). We scanned the elliptical cylinder acryl phantom (greatest diameter, 30 cm; smallest diameter, 20 cm; height, 10 cm) after filling a columnar hole (diameter, about 4 cm; height, 8 cm) through its elliptical center with a 4-fold dilution of contrast medium (iopamidol; Oypalomin 370; Fuji Pharma Co., Ltd, Tokyo, Japan).

### 2.2. Angiography unit and image reconstruction

We conducted 3D imaging using an AXIOM Artis zee BA (Siemens Healthcare GmbH, Forchheim, Germany) angiography unit with digital flat-panel system and applied parameters routinely used in clinical settings in our institution for abdominal 3D imaging on this unit (distance from source to axis of rotation, 75 cm; distance from source to image plane, 120 cm; rotation range, 200°; duration of rotation, 8 seconds; 397 projections; tube voltage and tube current-time product of each projection determined automatically by the system).

Each phantom was placed with its central axis overlapping the axis of the rotation and subjected to 3D imaging. The dose area products were 69.5 $Gy \times cm^2$ for the elliptical cylinder acrylic phantom and 15.8 $Gy \times cm^2$ for the Catphan phantom.

Three-dimensional imaging was calculated using Feldkamp algorithms from the multiple projection data in axial images with matrix of $512 \times 512$ pixels and 0.47-mm thickness at intervals of 0.47 mm and a display field of view measuring 23.9 cm.

The original axial images were transferred to a 3D-IIR server (SafeCT; Medic Vision, Tirat Carmel, Israel) for 3D-IIR at 5 settings used for abdominal examination: Sharp, Default, Soft+, Soft++, Soft+++, and we evaluated the quality of images reconstructed using each of the 6 reconstruction techniques.

### 2.3. Spatial resolution

To evaluate spatial resolution, we assessed modulation transfer functions (MTFs), targeting the hole containing diluted contrast medium through the center of the elliptical cylinder acrylic phantom. For this evaluation, we used 50 consecutive axial images for each of the 6 reconstruction techniques. To decrease the effect of noise, we averaged every 5 consecutive axial images for each reconstruction techniques and calculated MTFs on the averaged images using a circular edge method.[28,29] We also evaluated the 10% value of each MTF ($MTF_{10\%}$).

### 2.4. CT number linearity

To evaluate CT number linearity, we compared CT numbers in the same position among images reconstructed with each of the 6 reconstruction techniques. The sensitometry module (CTP 401) of the Catphan phantom comprises cylindrical rods (diameter, 1.25 cm) made from 4 different materials (Teflon, acrylic, low-density polyethylene, air). For each reconstruction technique, we measured CT numbers within a region of interest of about 0.68 $cm^2$ at the center of the 4 materials as well as the CT numbers of the background material on 10 consecutive images.

### 2.5. Noise of the system

To assess the magnitude and spatial frequency characteristics of image noise, we calculated the noise power spectra (NPS) of 10 consecutive reconstructed images of the uniformity module (CTP486) of the Catphan phantom for each of the 6 reconstruction techniques. We used image subtraction to remove low-frequency artifacts,[20,30,31] scanning the Catphan phantom twice to obtain 2 image sets for each reconstruction technique, and calculating the NPS using a radial frequency method. We minimized statistical error by utilizing the averaged value of the 10 spectra as the final NPS for images obtained using each of the reconstruction techniques.

### 2.6. Low-contrast resolution

To evaluate low-contrast resolution, we assessed the contrast-to-noise ratio (CNR) for a supraslice target of 15-mm diameter of 1.0% contrast on 10 consecutive reconstructed images of the low-contrast module (CTP515) of the Catphan phantom for each reconstruction technique.

### 2.7. Statistical analyses

We analyzed variance to test values of the $MTF_{10\%}$, the mean CT number measured on the sensitometry module of the Catphan phantom and the CNR, and used Scheffé tests for post hoc comparison of parameters, with $P < .05$ considered statistically significant. We used computer software (StatView 5.0 for windows; SAS Institute, Cary, NC) to perform these analyses.

## 3. Results

### 3.1. Spatial resolution

Figure 1 illustrates the modulation transfer function for each reconstruction technique and reflects excellent agreement among

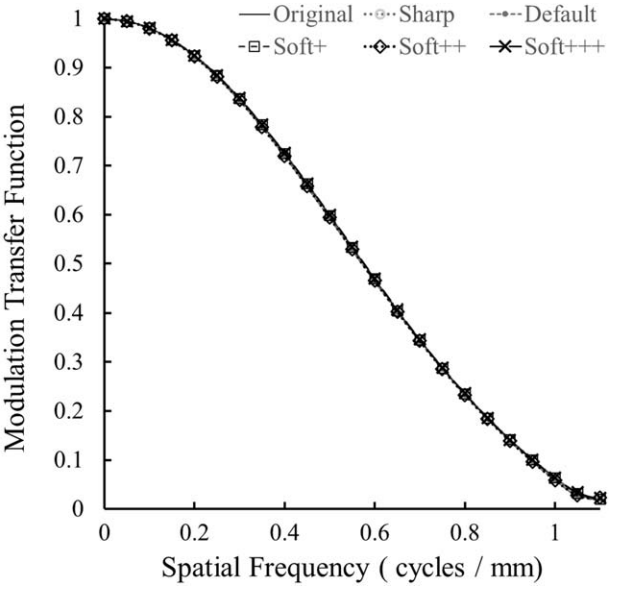


**Figure 1.** Modulation transfer function (MTF) of images obtained using 5 3D-IIR techniques and the original images acquired using customary reconstruction technique. The MTF curves of the 6 reconstruction techniques were almost the same.

**Table 1**

**$MTF_{10\%}$* of images obtained using customary and 5 3D-IIR* techniques.**

| | Original image using customary technique | Image using 3D-IIR | | | | |
|---|---|---|---|---|---|---|
| | | Sharp | Default | Soft+ | Soft++ | Soft+++ |
| $MTF_{10\%}$, cycles /mm | 0.960 ± 0.016 | 0.961 ± 0.016 | 0.965 ± 0.015 | 0.964 ± 0.017 | 0.966 ± 0.018 | 0.967 ± 0.016 |

* 3D-IIR = three-dimensional iterative image reconstruction, $MTF_{10\%}$ = 10% value of modulation transfer function.

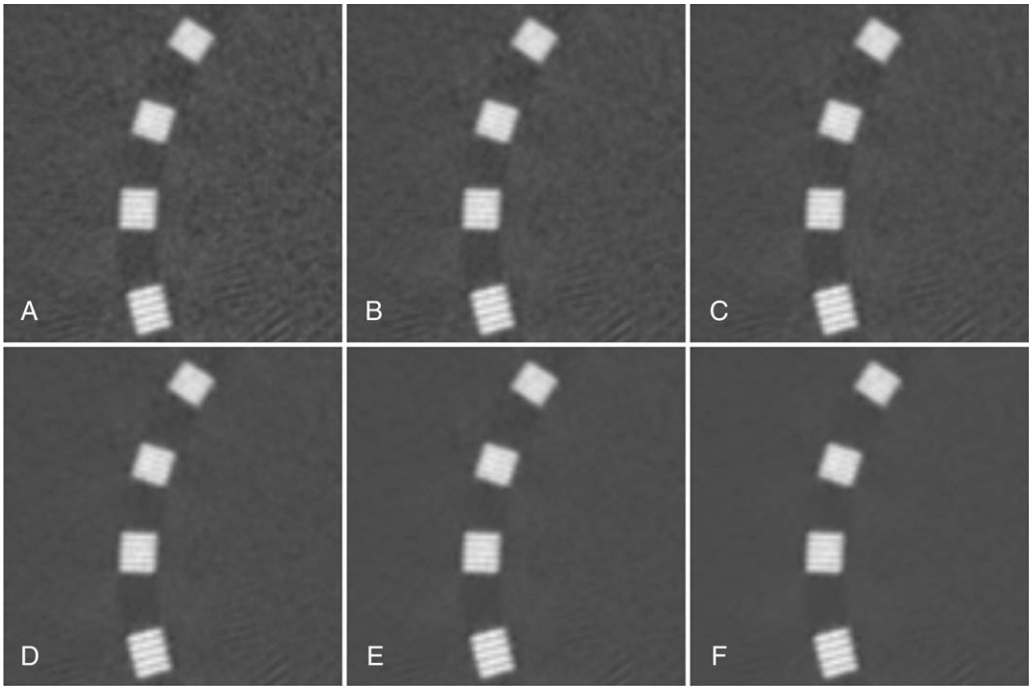


**Figure 2.** Bar patterns in the high resolution measurement module of the Catphan phantom (window width, 2000 Hounsfield units [HU]; window level, 500 HU). (A) Customary reconstruction technique; (B) 3D-IIR Sharp; (C) 3D-IIR Default; (D) 3D-IIR Soft+; (E) 3D-IIR Soft++; (F) 3D-IIR Soft+++. The patterns correspond with frequencies of 0.8, 0.9, 1.0, 1.1 cycles/mm (clockwise from the bottom).

the MTF curves obtained using the customary and 5 3D-IIR techniques. Table 1 summarizes the $MTF_{10\%}$ according to the 6 reconstruction techniques. We observed no significant difference ($P = .9275$) in $MTF_{10\%}$ among the 6 reconstruction techniques (Table 1). Figure 2 allows visual comparison of bar patterns of the high-resolution measurement with the 6 reconstruction techniques. The bar patterns showed no obvious change between images obtained using the 3D-IIR techniques and the original image acquired using customary reconstruction technique.

### 3.2. CT number linearity

We observed no interaction in any combination of factors ($P = .9976$) and no significant difference ($P = .4046$) in CT numbers among the 6 reconstruction techniques (Table 2).

### 3.3. Noise of the system

Figure 3 demonstrates uniform reduction of noise across the entire spatial frequency for the 3D-IIR images, with NPS curves of the 3D-IIR images and the original images all peaking at 0.30 cycles/mm.

**Table 2**

**CT* number of 5 kinds of materials measured using customary and 5 3D-IIR* techniques.**

| Material | Original image using customary technique | Image using 3D-IIR | | | | |
|---|---|---|---|---|---|---|
| | | Sharp | Default | Soft+ | Soft++ | Soft+++ |
| Teflon | 930.0 ± 1.3 | 929.2 ± 1.2 | 929.1 ± 1.3 | 928.8 ± 1.3 | 928.6 ± 1.4 | 928.4 ± 1.5 |
| Acrylic | 139.7 ± 2.1 | 138.7 ± 1.5 | 138.5 ± 1.3 | 138.1 ± 0.9 | 137.9 ± 0.7 | 137.6 ± 0.5 |
| Low-density polyethylene | −82.3 ± 3.5 | −82.4 ± 2.7 | −82.2 ± 2.4 | −81.8 ± 1.9 | −81.5 ± 1.6 | −81.2 ± 1.3 |
| Air | −856.1 ± 1.5 | −856.2 ± 1.5 | −856.4 ± 1.4 | −856.6 ± 1.5 | −856.6 ± 1.5 | −856.6 ± 1.5 |
| Background | 99.3 ± 6.7 | 98.1 ± 5.8 | 97.9 ± 5.5 | 97.4 ± 4.8 | 97.2 ± 4.5 | 96.9 ± 4.3 |

The CT number is given as the average ± standard deviation (HU).
* 3D-IIR = three-dimensional iterative image reconstruction, CT = computed tomography.

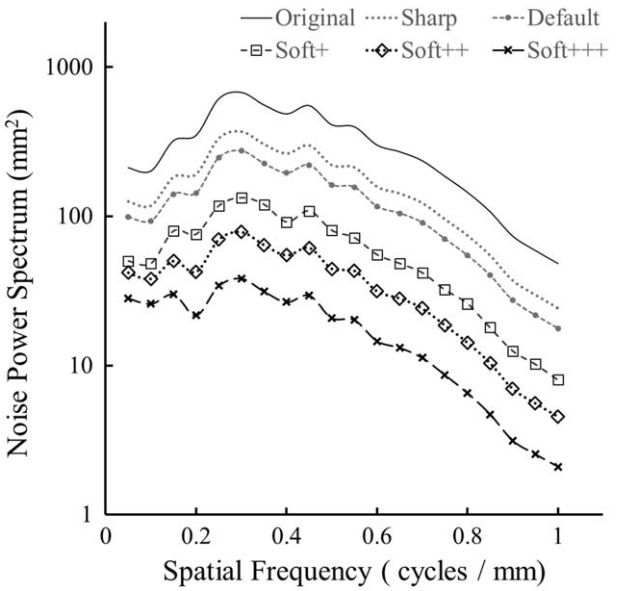


**Figure 3.** Noise power spectra of images obtained using 5 3D-IIR techniques and the original images acquired using customary reconstruction technique. The magnitude of noise of 3D-IIR images declined uniformly across the spatial frequency spectrum compared with noise in original images acquired by the customary reconstruction technique.

### *3.4. Low-contrast resolution*

Figure 4 demonstrates the improved visualization of the low-contrast targets utilizing the 3D-IIR settings, especially the sharper Soft++ and Soft+++ settings, using the low-contrast sensitivity module of the Catphan model with the 6 reconstruction techniques.

Table 3 summarizes the CNRs according to the 6 reconstruction techniques. Compared with the CNR obtained using the customary reconstruction technique, CNRs obtained using 3D-IIR settings, except the Sharp setting, were significantly improved (Sharp, $P = .1957$; Default, $P = .0042$; others, $P < .0001$), increasing in order from Sharp to Default to Soft+ to Soft++ and finally to Soft+++. CNRs differed significantly between Default and Soft+ ($P = .0003$), Soft+ and Soft++ ($P = .004$), and Soft++ and Soft+++ ($P < .0001$) but not between Sharp and Default ($P = .7366$).

## 4. Discussion

C-arm-based interventional CBCT presents 3D image information using a flat-panel-detector angiography system, offering superior spatial resolution to that of conventional CT because of the finer detector pitch of the CBCT but inferior low-contrast resolution as a result of more scattered radiation.[2,8,17–19] The advancement of interventional radiology requires the acquisition of accurate 3D image information,[2] and thus the higher quality of C-arm-based interventional CBCT images is desired, especially with regard to detection of objects with low contrast.

Various IR techniques have been developed for use in conventional CT in a clinical setting,[21,32] and their utility in increasing low-contrast resolution has been reported.[20,22–25,32,33] The 3D-IIR system allows the processing of images for iterative reconstruction in image space and can be used with scanners from any vendor.[30,34–38] It employs an iterative algorithm to reconstruct volume data to process DICOM image data for denoising based on the knowledge of statistics of the CT noise distribution.[35,36] The 3D-IIR system has been reported

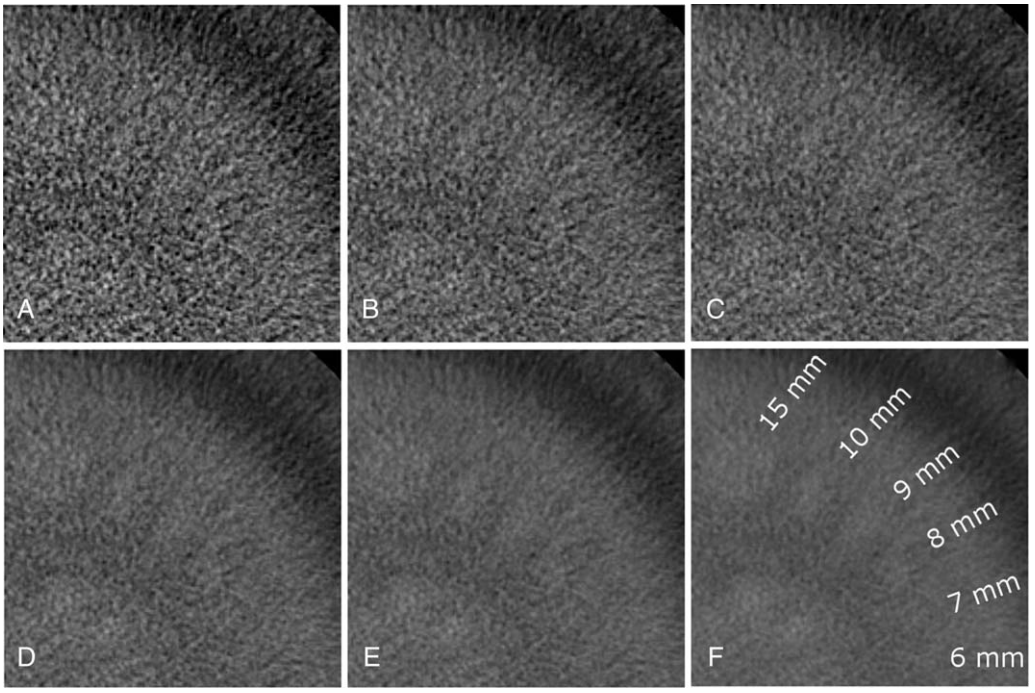


**Figure 4.** Targets of contrast level with 1.0% in the low-contrast sensitivity module of a Catphan (window width, 150 Hounsfield units [HU]; window level, 50 HU). (A) Customary reconstruction technique; (B) 3D-IIR Sharp; (C) 3D-IIR Default; (D) 3D-IIR Soft+; (E) 3D-IIR Soft++; (F) 3D-IIR Soft+++. All images are the average of 5 consecutive images reconstructed by the 6 reconstruction techniques. The diameters of the targets are 15, 10, 9, 8, 7, 6 mm (clockwise from top). The target of 10-mm diameter is unclear on the image obtained with the original reconstruction technique, but visualization of the low-contrast targets improved using the 3D-IIR techniques, especially with the Soft++ and Soft+++ settings. Nothing unfamiliar was apparent on images obtained using 3D-IIR.

**Table 3**

**Contrast-to-noise ratio using customary and 5 3D-IIR* techniques.**

| | Original image using customary technique | Image using 3D-IIR | | | | |
|---|---|---|---|---|---|---|
| | | Sharp | Default | Soft+ | Soft++ | Soft+++ |
| Contrast-to-noise ratio | 0.294 ± 0.090 | 0.392 ± 0.087 | 0.452 ± 0.086 | 0.642 ± 0.078 | 0.829 ± 0.072 | 1.178 ± 0.064 |

* 3D-IIR = three-dimensional iterative image reconstruction.

capable to reduce noise of conventional CT images with maintenance of structural detail,[34,35] but we believe this is the first study to evaluate its performance in the acquisition of C-arm-based interventional CBCT images.

The effects of IR techniques on NPS have been reported using conventional CT,[21,30,39] and their use has been reported to decrease the area under the NPS curve that corresponds with the level of image noise.[20,21,34,37,39] Our use of 3D-IIR for C-arm-based interventional CBCT in this study also decreased this area. In contrast, the peak of the NPS curve shifts toward lower frequencies in conventional CT with many kinds of IR techniques,[20,21,39] which means that the noise of rough textures increases relatively, yielding an unfamiliar mottled appearance and loss of low-contrast spatial resolution.[21] However, we observed no such shift of the NPS curve or unfamiliar visual appearance using 3D-IIR (Fig. 4), which was consistent with Padole's report of the absence of blotchy appearance on images of conventional CT obtained using a submillisievert dose of radiation with 3D-IIR.[36] In this study, 3D-IIR preserved CT number linearity and decreased noise, especially with the use of Soft++ and Soft+++ settings, which led to increased CNR and subsequent improved visualization of objects with low contrast (Fig. 4).

Just as NPS is one of the most common metrics for X-ray-based systems to describe the magnitude and spatial frequency characteristics of image noise,[21,30,40,41] MTF is one of the most common metrics for those systems to describe spatial resolution.[21,29] The MTF of images obtained using IR techniques and conventional CT can depend on contrast and radiation dose as the result of a nonlinear process.[29] To evaluate spatial resolution obtained using IR techniques, conventional techniques for measuring MTF, such as the wire method, are unsuitable because these techniques are used for images of highly dense material with very low noise.[29] On the contrary, measurement of MTF using a circular edge method to evaluate spatial resolution using IR depends on neither contrast nor radiation dose.[28,29] In the current evaluation of spatial resolution simulating that obtained in a clinical setting, the use of 3D-IIR did not obviously affect MTF measurement using a circular edge method, which suggests that noise reduction achieved using 3D-IIR preserves spatial resolution.

The radiation exposure dose of C-arm-based interventional CBCT varies by diagnostic application and corresponding exposure setting,[8,42] and studies in phantoms have reported effective doses of only a few mSv.[8,42–45] However, a single interventional procedure can require the repetition of C-arm-based CBCT, so it is desirable to minimize the exposure dose. The level of image noise in C-arm-based CBCT obtained using standard Feldkamp algorithms is proportional to the tube current,[8] and our observation of reduced noise with preservation of spatial resolution using 3D-IIR suggests the potential of this IR technique to reduce radiation dose for C-arm-based interventional CBCT. On the contrary, in conventional CT, dose reduction using IR algorithms can cause loss of low-contrast spatial resolution and coarsening of noise texture.[21] Therefore, the same phenomenon can be observed for dose reduction using IR algorithms in C-arm-based interventional CBCT.

Our study is limited by our use of an angiography unit from only a single vendor, but the 3D-IIR system can be applied in the acquisition of C-arm-based interventional CBCT images using units from other vendors, and further study using other types of angiography units may be warranted to confirm our results. In addition, we used images of phantoms and not patients. C-arm-based interventional CBCT images are susceptible to artifacts such as photon starvation artifacts, beam hardening, and metal artifacts,[46] and these artifacts sometimes decrease the quality of clinical images of patients. However, it is known that image-based IRs are not effective to decrease these artifacts.[21] Further studies of images of patients are required to evaluate the effects of such artifacts on the quality of images reconstructed using the 3D-IIR system.

In conclusion, the use of 3D-IIR in the acquisition of abdominal C-arm-based interventional CBCT can significantly reduce image noise and improve visualization of targets with low contrast while maintaining spatial resolution, yielding images of higher quality than those obtained by customary methods that may increase the safety and efficacy of interventional radiology.

## Acknowledgments

We thank NAGASE & CO., LTD, for allowing us free use of SafeCT.

## Author contributions

**Conceptualization:** Shigeru Suzuki, Yoshiaki Katada.
**Data curation:** Shigeru Suzuki, Tomoko Takayanagi, Yuzo Yamamoto.
**Formal analysis:** Shigeru Suzuki, Hiroo Wada.
**Investigation:** Shigeru Suzuki, Tomoko Takayanagi, Haruto Sugawara, Takuya Ishikawa, Yuzo Yamamoto.
**Methodology:** Shigeru Suzuki, Hiroo Wada.
**Software:** Shigeru Suzuki.
**Supervision:** Shigeru Suzuki, Yoshiaki Katada, Hiroo Wada.
**Visualization:** Shigeru Suzuki.
**Writing—original draft:** Shigeru Suzuki, Yuzo Yamamoto.
**Writing—review and editing:** Shigeru Suzuki, Yoshiaki Katada, Tomoko Takayanagi, Haruto Sugawara, Takuya Ishikawa, Hiroo Wada.

## References

[1] Feldkamp LA, Davis LC, Kress JW. Practical cone-beam algorithm. J Opt Soc Am A 1984;1:612–9.
[2] Grass M, Guillemaud R, Rasche V. Grangeat P. Interventional x-ray volume tomography. Tomography London, UK: ISTE/Wiley; 2009;287–306.
[3] Saint-Felix DM, Picard CL, Ponchut C, Romeas R, Rougee A, Trousset YL. Kim Y. Three dimensional x-ray angiography: first in-vivo results with a new system. Proceedings of SPIE: Medical Imaging 1993—Image Capture, Formatting, and Display. vol. 1897 Bellingham, Washington: SPIE–The International Society for Optical Engineering; 1993;90–8.

[4] Grass M, Koppe R, Klotz E, et al. Three-dimensional reconstruction of high contrast objects using C-arm image intensifier projection data. Comput Med Imaging Graph 1999;23:311–21.
[5] Wang T, Nakamoto K, Zhang H, et al. Reweighted anisotropic total variation minimization for limited-angle CT reconstruction. IEEE Trans Nucl Sci 2017;64:2742–60.
[6] Müller K, Datta S, Ahmad M, et al. Interventional dual-energy imaging-feasibility of rapid kV-switching on a C-arm CT system. Med Phys 2016;43:5537.
[7] Martin R, Ahmad M, Hugo G, et al. Iterative volume of interest based 4D cone-beam CT. Med Phys 2017;44:6515–28.
[8] Rehanni MM, Gupta R, Bartling S, et al. I.C.R.P.Radiological protection in cone beam computed tomography (CBCT). Ann ICRP 2015;44:9–127.
[9] McKay T, Ingraham CR, Johnson GE, et al. Cone-beam CT with fluoroscopic overlay versus conventional CT guidance for percutaneous abdominopelvic abscess drain placement. J Vasc Interv Radiol 2016;27:52–7.
[10] Racadio JM, Babic D, Homan R, et al. Live 3D guidance in the interventional radiology suite. AJR Am J Roentgenol 2007;189:W357–64.
[11] Lucatelli P, Argirò R, Bascetta S, et al. Single injection dual phase CBCT technique ameliorates results of trans-arterial chemoembolization for hepatocellular cancer. Transl Gastroenterol Hepatol 2017;24:83.
[12] Lucatelli P, Argirò R, Ginanni Corradini S, et al. Comparison of image quality and diagnostic performance of cone-beam CT during drug-eluting embolic transarterial chemoembolization and multidetector CT in the scinoma. J Vasc Interv Radiol 2017;28:978–86.
[13] Lucatelli P, Corona M, Argirò R, et al. Impact of 3D rotational angiography on liver embolization procedures: review of technique and applications. Cardiovasc Intervent Radiol 2015;38:523–35.
[14] Orth RC, Wallace MJ, Kuo MD. Technology Assessment Committee of the Society of Interventional Radiology. C-arm cone-beam CT: general principles and technical considerations for use in interventional radiology. J Vasc Interv Radiol 2008;19:814–20.
[15] Busser WM, Braak SJ, Fütterer JJ, et al. Cone beam CT guidance provides superior accuracy for complex needle paths compared with CT guidance. Br J Radiol 1030;86:20130310.
[16] Abi-Jaoudeh N, Venkatesan AM, Van der Sterren W, et al. Clinical experience with cone-beam CT navigation for tumor ablation. J Vasc Interv Radiol 2015;26:214–9.
[17] Orth RC, Wallace MJ, Kuo MD. Technology Assessment Committee of the Society of Interventional Radiology. C-arm cone-beam CT: general principles and technical considerations for use in interventional radiology. J Vasc Interv Radiol 2009;20:S538–44.
[18] Paul J, Jacobi V, Farhang M, et al. Radiation dose and image quality of X-ray volume imaging systems: cone-beam computed tomography, digital subtraction angiography and digital fluoroscopy. Eur Radiol 2013;23:1582–93.
[19] Gonzalez-Guindalini FD, Ferreira Botelho MP, Töre HG, et al. MDCT of chest, abdomen, and pelvis using attenuation-based automated tube voltage selection in combination with iterative reconstruction: an intrapatient study of radiation dose and image quality. AJR Am J Roentgenol 2013;201:1075–82.
[20] Marin D, Nelson RC, Schindera ST, et al. Low-tube-voltage, high-tube-current multidetector abdominal CT: improved image quality and decreased radiation dose with adaptive statistical iterative reconstruction algorithm—initial clinical experience. Radiology 2010;254:145–53.
[21] Ehman EC, Yu L, Manduca A, et al. Methods for clinical evaluation of noise reduction techniques in abdominopelvic CT. Radiographics 2014;34:849–62.
[22] Deák Z, Grimm JM, Treitl M, et al. Filtered back projection, adaptive statistical iterative reconstruction, and a model-based iterative reconstruction in abdominal CT: an experimental clinical study. Radiology 2013;266:197–206.
[23] Schindera ST, Odedra D, Raza SA, et al. Iterative reconstruction algorithm for CT: can radiation dose be decreased while low-contrast detectability is preserved? Radiology 2013;269:511–8.
[24] Hara AK, Paden RG, Silva AC, et al. Iterative reconstruction technique for reducing body radiation dose at CT: feasibility study. AJR Am J Roentgenol 2009;193:764–71.
[25] Singh S, Kalra MK, Gilman MD, et al. Adaptive statistical iterative reconstruction technique for radiation dose reduction in chest CT: a pilot study. Radiology 2011;259:565–73.
[26] Cao Q, Zbijewski W, Sisniega A, et al. Multiresolution iterative reconstruction in high-resolution extremity cone-beam CT. Phys Med Biol 2016;61:7263–81.
[27] Tilley S, Siewerdsen JH, Stayman JW. Model-based iterative reconstruction for flat-panel cone-beam CT with focal spot blur, detector blur, and correlated noise. Phys Med Biol 2016;61:296–319.
[28] Takenaga T, Katsuragawa S, Goto M, et al. Modulation transfer function measurement of CT images by use of a circular edge method with a logistic curve-fitting technique. Radiol Phys Technol 2015;8:53–9.
[29] Richard S, Husarik DB, Yadava G, et al. Towards task-based assessment of CT performance: system and object MTF across different reconstruction algorithms. Med Phys 2012;39:4115–22.
[30] Dolly S, Chen HC, Anastasio M, et al. Practical considerations for noise power spectra estimation for clinical CT scanners. J Appl Clin Med Phys 2016;17:392–407.
[31] Zhou Z, Gao F, Zhao H, et al. Techniques to improve the accuracy of noise power spectrum measurements in digital x-ray imaging based on background trends removal. Med Phys 2011;38:1600–10.
[32] Geyer LL, Schoepf UJ, Meinel FG, et al. State of the art: iterative CT reconstruction techniques. Radiology 2015;276:339–57.
[33] Patino M, Fuentes JM, Singh S, et al. Iterative reconstruction techniques in abdominopelvic CT: technical concepts and clinical implementation. AJR Am J Roentgenol 2015;205:W19–31.
[34] Khawaja RD, Singh S, Blake M, et al. Ultralow-dose abdominal computed tomography: comparison of 2 iterative reconstruction techniques in a prospective clinical study. J Comput Assist Tomogr 2015;39:489–98.
[35] Pourjabbar S, Singh S, Singh AK, et al. Preliminary results: prospective clinical study to assess image-based iterative reconstruction for abdominal computed tomography acquired at 2 radiation dose levels. J Comput Assist Tomogr 2014;38:117–22.
[36] Padole A, Singh S, Ackman JB, et al. Submillisievert chest CT with filtered back projection and iterative reconstruction techniques. AJR Am J Roentgenol 2014;203:772–81.
[37] Pourjabbar S, Singh S, Kulkarni N, et al. Dose reduction for chest CT: comparison of two iterative reconstruction techniques. Acta Radiol 2015;56:688–95.
[38] Padole A, Digumarthy S, Flores E, et al. Assessment of chest CT at CTDIvol less than 1 mGy with iterative reconstruction techniques. Br J Radiol 2017;90:20160625.
[39] Solomon J, Mileto A, Ramirez-Giraldo JC, et al. Diagnostic performance of an advanced modeled iterative reconstruction algorithm for low-contrast detectability with a third-generation dual-source multidetector CT scanner: potential for radiation dose reduction in a multireader study. Radiology 2015;275:735–45.
[40] Boedeker KL, Cooper VN, McNitt-Gray MF. Application of the noise power spectrum in modern diagnostic MDCT: part I. Measurement of noise power spectra and noise equivalent quanta. Phys Med Biol 2007;52:4027–46.
[41] Boedeker KL, McNitt-Gray MF. Application of the noise power spectrum in modern diagnostic MDCT: part II. Noise power spectra and signal to noise. Phys Med Biol 2007;52:4047–61.
[42] Floridi C, Radaelli A, Abi-Jaoudeh N, et al. C-arm cone-beam computed tomography in interventional oncology: technical aspects and clinical applications. Radiol Med 2014;119:521–32. (Note: This article has been corrected. See Radiol Med. 2015 April; 120:406.).
[43] Bai M, Liu B, Mu H, et al. The comparison of radiation dose between C-arm flat-detector CT (DynaCT) and multi-slice CT (MSCT): a phantom study. Eur J Radiol 2012;81:3577–80.
[44] Koyama S, Aoyama T, Oda N, et al. Radiation dose evaluation in tomosynthesis and C-arm cone-beam CT examinations with an anthropomorphic phantom. Med Phys 2010;37:4298–306.
[45] Suzuki S, Yamaguchi I, Kidouchi T, et al. Evaluation of effective dose during abdominal three-dimensional imaging for three flat-panel-detector angiography systems. Cardiovasc Intervent Radiol 2011;34:376–82.
[46] Tacher V, Radaelli A, Lin M, et al. How I do it: cone-beam CT during transarterial chemoembolization for liver cancer. Radiology 2015;274:320–34.